

Near-field measurement of spectral anisotropy and optical absorption of isolated ZnO nanorod single-quantum-well structures

Takashi Yatsui^{a)} and Motoichi Ohtsu^{b)}

Solution-Oriented Research for Science and Technology, Japan Science and Technology Agency, Machida, Tokyo, 194-0004 Japan

Jinkyong Yoo, Sung Jin An, and Gyu-Chul Yi

National CRI Center for Semiconductor Nanorods and Department of Materials Science and Engineering, Pohang University of Science and Technology (POSTECH), San 31 Hyoja-dong, Pohang, Gyeongbuk 790-784, Korea

(Received 3 February 2005; accepted 10 June 2005; published online 11 July 2005)

We report low-temperature near-field spectroscopy of isolated ZnO/ZnMgO single-quantum-well structures (SQWs) on the end of ZnO nanorod to define their potential for nanophotonics. First, absorption spectra of isolated ZnO/ZnMgO nanorod SQWs with the Stokes shift as small as 3 meV and very sharp photoluminescent peaks indicate that the nanorod SQWs are of very high optical quality. Furthermore, we performed polarization spectroscopy of isolated ZnO SQWs, and observed valence-band anisotropy of ZnO SQWs in photoluminescence spectra directly. Since the exciton in a quantum structure is an ideal two-level system with long coherence times, our results provide criteria for designing nanophotonic devices. © 2005 American Institute of Physics.

[DOI: 10.1063/1.1990247]

ZnO nanocrystallites are a promising material for realizing nanometer-scale photonic devices,¹ i.e., nanophotonic devices, at room temperature, owing to their large exciton binding energy²⁻⁴ and large oscillator strength.⁵ Furthermore, the recent demonstration of semiconductor nanorod quantum-well structures enables us to fabricate nanometer-scale electronic and photonic devices on single nanorods.⁶⁻⁹ Recently, ZnO/ZnMgO nanorod heterostructures were fabricated and the quantum confinement effect even from the single-quantum-well structures (SQWs) was observed.¹⁰ Near-field spectroscopy has made a remarkable contribution to investigations of the optical properties in nanocrystallite,¹¹ and has resulted in the observation of nanometer-scale optical images, such as the local density of exciton states.¹² However, reports on semiconductor quantum structure are limited to naturally formed quantum dots (QDs).¹²⁻¹⁴ Here we report low-temperature near-field spectroscopy of artificially fabricated ZnO SQWs on the end of a ZnO nanorod.

ZnO/ZnMgO SQWs were fabricated on the ends of ZnO stems with a mean diameter of 40 nm and a length of 1 μm using catalyst-free metalorganic vapor phase epitaxy, in which the ZnO nanorods were grown vertically from a sapphire (0001) substrate in the c orientation.^{10,15} The Mg concentration in the ZnMgO layers averaged 20 at. %. Two samples were prepared for this study: their ZnO well layer thickness L_w , were 2.5 and 3.75 nm, while the thicknesses of the ZnMgO bottom and top barrier layers in the SQWs were fixed at 60 and 18 nm, respectively. After growing the ZnO/ZnMgO nanorod SQWs, they were dispersed so that they were laid down on a flat sapphire substrate to isolate them from each other [Fig. 1(a)].

The far-field photoluminescence (PL) spectra were obtained using a He–Cd laser ($\lambda=325$ nm) before dispersion of the ZnO/ZnMgO nanorod SQWs. The emission signal was

collected with the acromatic lens ($f=50$ mm). To confirm that the optical qualities of individual ZnO/ZnMgO SQWs were sufficiently high, we used a collection-mode near-field optical microscope (NOM) using a He–Cd laser ($\lambda=325$ nm) for excitation, and a UV fiber probe with an aperture diameter of 30 nm. The excitation source was focused on a nanorod sample laid on the substrate with a spot size approximately 100 μm in diameter. The PL signal was collected with the fiber probe, and detected using a cooled charge coupled device through a monochromator. The fiber probe was kept in close proximity to the sample surface (~ 5 nm) using the shear-force feedback technique. The polarization of the incident light was controlled with a $\lambda/2$

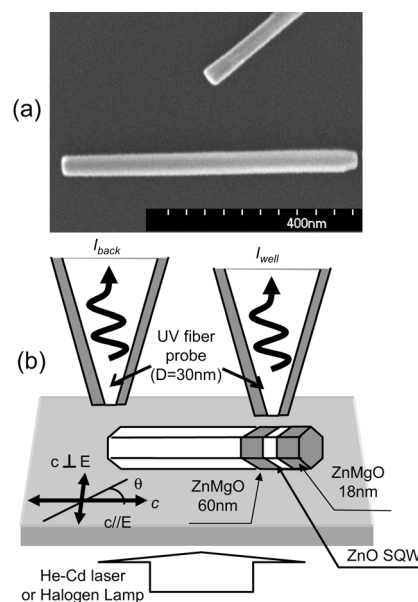


FIG. 1. Schematic of experimental setup for near-field PL spectroscopy. (a) Scanning electron micrograph of the dispersed ZnO/ZnMgO SQWs. (b) Schematic of ZnO/ZnMgO SQWs on the ends of ZnO nanorods. c : c axis of the ZnO stem. θ : angle between the ZnO stem and the direction of incident light polarization.

^{a)}Electronic mail: yatsui@ohtsu.jst.go.jp

^{b)}Also at: School of Engineering, The University of Tokyo, Bunkyo-ku, Tokyo, 113-8656 Japan.

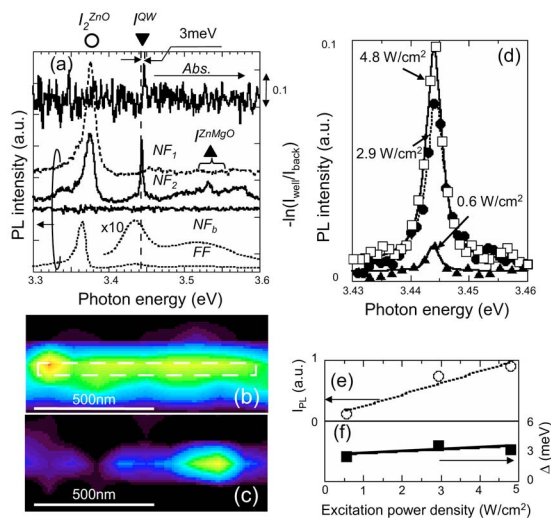


FIG. 2. (Color online) Near-field PL and absorption spectroscopy of isolated ZnO SQWs ($L_w=3.75$ nm) at 15 K. (a) NF_1 , NF_2 : near-field PL spectra. NF_b : background noise. Abs.: near-field absorption spectrum. FF: far-field PL spectrum of vertically aligned ZnO SQWs ($L_w=3.75$ nm). NOM images of isolated ZnO SQWs obtained at (b) 3.375 and (c) 3.444 eV. The rectangle shown in dashed white lines indicates the position of the ZnO stem. (d) Near-field PL spectra of isolated ZnO SQWs at excitation densities ranging from 0.6 to 4.8 W/cm². The integrated PL intensity I_{PL} (e) and homogeneous linewidths Δ (f) as a function of the excitation power density.

wave plate. In contrast to the naturally formed QD structure (a high monolayer island formed in a narrow quantum well), the barrier and cap layers laid on the substrate allowed the probe tip access to the PL source, which reduced carrier diffusion in the ZnO SQWs and the subsequent linewidth broadening, thereby achieving a high spatial and spectral resolution. In addition to the PL measurements, absorption spectra were obtained using a halogen lamp, where the absorption was defined by the ratio I_{well}/I_{back} between the signal intensities transmitted through the well layer (I_{well}) and substrate (I_{back} , 50 nm apart from the well layer) [Fig. 1(b)]. The absorption signal was collected with the same fiber probe with an aperture diameter of 30 nm. Since the ZnMgO layers are much thicker than that of the well layer (~ 3 nm), any difference in the transmission signals between I_{well} and I_{back} was not detected, which resulted in no detection of the absorption peak originating from the ZnMgO layers.

As a preliminary near-field spectroscopy experiment of the ZnO SQWs, we obtained near-field PL spectra of the ZnO SQWs with $L_w=3.75$ nm [Fig. 2(a)] obtained with polarization perpendicular to the c axis [$\theta=90^\circ$ in Fig. 1(b)]. Two typical spectra are shown, one with a single peak at 3.375 eV (NF_1) and the other with several sharp peaks around 3.375, 3.444, and 3.530 eV (NF_2), while NF_b is a background spectra [Fig. 2(a)]. Several conclusions can be drawn from these spectral profiles. First, comparison with the far-field PL spectrum [FF: dashed curve in Fig. 2(a)] showed that the emission peak I_{2a}^{ZnO} at 3.375 eV was suppressed, and I^{QW} (3.444 eV) and I_{2a}^{ZnMgO} (3.530 eV) were enhanced in NF_2 , indicating that peaks I_{2a}^{ZnO} and I_{2a}^{ZnMgO} originated from the ZnO stem and ZnMgO layers, respectively. Second, since the peak position of I^{QW} was consistent with the theoretical prediction (3.430 eV) using the finite square-well potential of the quantum confinement effect in the ZnO well layer for $L_w=3.75$ nm, we concluded that peak I^{QW} originated from the ZnO SQWs. The theoretical calculation

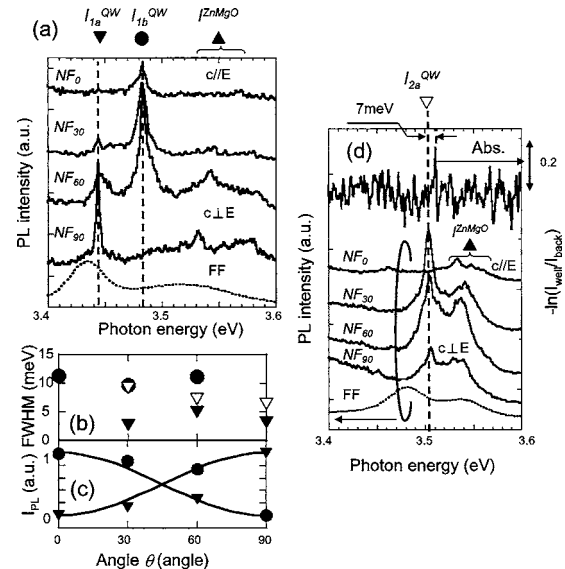


FIG. 3. Polarization dependence of near-field PL spectra of isolated ZnO SQWs obtained at 15 K. (a) NF_θ , FF: near-field and far-field PL spectra of isolated ZnO SQWs ($L_w=3.75$ nm) for $\theta=0^\circ, 30^\circ, 60^\circ,$ and 90° . (b) Solid triangles and circles are the polarization dependence of the linewidth of I_{1a}^{QW} and I_{1b}^{QW} , respectively in (a). Open triangles are the polarization dependence of linewidth of I_{2a}^{QW} in (d). (c) Solid triangles and circles are the integrated PL intensities (I_{PL}) of I_{1a}^{QW} and I_{1b}^{QW} , respectively, normalized to the total PL intensities ($I_{1a}^{QW} + I_{1b}^{QW}$). (d) NF_θ , FF: near-field and far-field PL spectra, respectively, of isolated ZnO SQWs ($L_w=2.5$ nm). Abs.: absorption spectrum.

used $0.28m_0$ and $1.8m_0$ as the effective masses of an electron and hole in ZnO, respectively, at a ratio of conduction- and valence-band offsets ($\Delta E_c/\Delta E_v$) of 9, and a band-gap offset (ΔE_g) of 250 meV.¹⁰ The spatial distributions of the near-field PL intensity of peaks I_{2a}^{ZnO} and I^{QW} [Figs. 2(b) and 2(c)] supported the postulate that the blueshifted emission was confined to the end of the ZnO stem. Third, the spectral width (3 meV) of peak I^{QW} was much narrower than those of the far-field PL spectra (40 meV). To estimate the homogeneous linewidth of isolated ZnO SQWs, we observed the power dependence of the near-field PL spectra [Fig. 2(d)] by varying the excitation power densities from 0.6 to 4.8 W/cm². The shape of each spectrum was fitted using the Lorentzian function indicated by the solid curve. Figures 2(e) and 2(f) show the integrated PL intensity (I_{PL}) and linewidth (Δ) of the fitted Lorentzian, which increased linearly and remained constant around 3 meV, respectively. These results indicate that emission peak I^{QW} represented the emission from a single-exciton state in ZnO SQWs and that the linewidth was governed by the homogeneous broadening. Fourth, the Stokes shift of 3 meV [Fig. 2(a)] was much smaller than the reported value (50 meV) in ZnO/ZnMgO superlattices.^{16,17} The small Stokes shift may result from the decreased piezoelectric polarization effect by the fully relaxed strain for the ZnO/ZnMgO nanorod quantum structures in contrast to the two-dimensional (2D) ZnO/ZnMgO heteroepitaxial multiple layers are strongly supported by the theoretical calculation on the double barrier InAs/InP nanorod heterostructures.¹⁸

Based on these experiments, a major investigation of the optical properties of isolated ZnO SQWs was performed by analyzing the polarization-dependent PL spectrum of isolated ZnO SQWs ($L_w=3.75$ nm). As shown in Fig. 3(a), NF_0 is a near-field PL spectrum obtained with parallel polarization with respect to the c axis, $\theta=0^\circ$, and this exhibits a new peak

I_{1b}^{QW} at 3.483 eV, which is out of peak in the far-field spectrum (3.435 eV \pm 20 meV). Peak I_{1a}^{QW} is the same as I^{QW} in Fig. 2(a).

As the ZnO has valence-band anisotropy owing to the wurtzite crystal structure, the operator corresponds to the $\Gamma_5(\Gamma_1)$ representation when the electric vector \mathbf{E} of the incident light is perpendicular (parallel) to the crystalline c axis, respectively. By considering the energy difference between Γ_5 and Γ_1 in the center of the zone around 40 meV for bulk material,^{5,19,20} and the direction of the incident light polarization with respect to the c axis, emission peaks I_{1a}^{QW} and I_{1b}^{QW} in Fig. 3(a) are allowed for the exciton from Γ_5 and Γ_1 , respectively. This observation of a Γ_1 exciton in a PL spectrum originates from the enhancement of the exciton binding energy owing to the quantum confinement effect⁴ because the exciton binding energy of the emission from Γ_1 (50–56 meV) (see Refs. 20 and 21) is comparable to that from Γ_5 (60 meV). Furthermore, in contrast to the bulk ZnO film, our sample configuration using laid ZnO nanorod SQWs has realized π polarization ($\theta=0^\circ$), allowing the detection of the emission from the Γ_1 exciton. The homogeneous linewidth of emission peak I_{1a}^{QW} (Γ_5) is in the range 3–5 meV, while that of I_{1b}^{QW} (Γ_1) is 9–11 meV [Fig. 3(b)]. This difference is attributed to the degeneracy of the transition of the Γ_1 exciton with continuum and to the contribution of the residual strain field, and results in sensitive dependence of the Γ_1 exciton on the strain, as reported in the GaN.²² The solid triangles and circles in Fig. 3(c) shows the respective normalized integrated PL intensity at I_{1a}^{QW} and I_{1b}^{QW} , respectively, which are in good agreement with the sine-squared and cosine-squared functions represented by the solid curves. These results indicate that emission peaks I_{1a}^{QW} and I_{1b}^{QW} originate from unidirectional transition dipoles that are orthogonal to each other.

To study the linewidth broadening mechanism, Fig. 3(d) shows the polarization-dependent near-field PL spectra (NF₀–NF₉₀) and absorption spectrum obtained for isolated ZnO SQWs with a thinner well layer ($L_w=2.5$ nm). In NF₀–NF₉₀, the emission peaks I^{ZnMgO} around 3.535 eV originate from the ZnMgO layers. Emission peak I_{2a}^{QW} originates from the Γ_5 exciton in the SQWs, as was the case for I_{1a}^{QW} in Fig. 3(a), since the position of peak I_{2a}^{QW} (3.503 eV) is comparable to that of the dominant peak in the far-field PL spectra (3.480 eV) and the theoretical prediction (3.455 eV) using the finite square-well potential of the quantum confinement effect in the ZnO well layer. In comparison to ZnO SQWs with $L_w=3.75$ nm, however, emission peak I_{2a}^{QW} had a broader linewidth (7–10 meV), which is attributed to the shorter exciton dephasing time. In the nanocrystallite where the excitons are quantized, the linewidth should be determined by the exciton dephasing time. Such dephasing arises from the collisions of the excitons at the irregular surface, so that the linewidth is d^{-2} (d is the effective size of the quantum structure).²³ The observed well-width dependence of the spectral linewidth, $3.75^{-2}/2.5^{-2}\sim 3/7$, and the Stokes shift of 7 meV [see Fig. 3(c)] larger than that for $L_w=3.75$ nm (3 meV) are supported by this dephasing mechanism quantitatively. Although emission peak I_{2a}^{QW} was suppressed for $\theta=0^\circ$, no peaks corresponding to the Γ_1 exciton in SQWs were detected owing to the reduction of the exciton binding energy, since the peak energy of Γ_1 for the ZnO SQWs with

$L_w=2.5$ nm is comparable with that of ZnMgO.

The results shown here provide criteria for realizing nanophotonic devices using a two-level system.^{24,25} As a representative device, a nanophotonic switch can be realized by controlling the dipole forbidden optical energy transfer among resonant energy levels in nanometer-scale QD via an optical near field.²⁶ Since the switching dynamics was already confirmed using CuCl quantum cubes,²⁶ the success of near-field PL and absorption measurement of isolated SQWs described above is a promising step toward designing a nanophotonic switch and related devices.

The authors are grateful to Drs. I. Banno (Yamanashi University) and S. Sangu (Ricoh Company, Ltd.) for many fruitful discussions. The work at POSTECH was supported by the National Creative Research Initiative Project, Korea and the AOARD 04–49 (Quotation No. FA5209–04–T0254).

¹M. Ohtsu, K. Kobayashi, T. Kawazoe, S. Sangu, and T. Yatsui, IEEE J. Sel. Top. Quantum Electron. **8**, 839 (2002).

²A. Ohtomo, K. Tamura, M. Kawasaki, T. Makino, Y. Segawa, Z. K. Tang, G. K. L. Wong, Y. Matsumoto, and H. Koinuma, Appl. Phys. Lett. **77**, 2204 (2000).

³M. H. Huang, S. Mao, H. Feick, H. Yan, Y. Wu, H. Kind, E. Weber, R. Russo, and P. Yang, Science **292**, 1897 (2001).

⁴H. D. Sun, T. Makino, Y. Segawa, M. Kawasaki, A. Ohtomo, K. Tamura, and H. Koinuma, J. Appl. Phys. **91**, 1993 (2002).

⁵D. C. Reynolds, D. C. Look, B. Jogai, C. W. Litton, G. Cantwell, and W. C. Harsch, Phys. Rev. B **60**, 2340 (1999).

⁶Y. Wu, R. Fan, and P. Yang, Nano Lett. **2**, 83 (2002).

⁷M. T. Björk, B. J. Ohlsson, C. Thelander, A. I. Persson, K. Deppert, L. R. Wallenberg, and L. Samuelson, Appl. Phys. Lett. **81**, 4458 (2003).

⁸M. S. Gudiksen, L. J. Lauhon, J. Wang, D. C. Smith, and C. M. Lieber, Nature (London) **415**, 617 (2002).

⁹W. I. Park, G.-C. Yi, M. Kim, and S. J. Pennycook, Adv. Mater. (Weinheim, Ger.) **15**, 526 (2003).

¹⁰W. I. Park, S. J. An, J. L. Yang, G.-C. Yi, S. Hong, T. Joo, and M. Kim, J. Phys. Chem. B **108**, 15457 (2004).

¹¹K. Matsuda, T. Saiki, S. Nomura, M. Mihara, and Y. Aoyagi, Appl. Phys. Lett. **81**, 2291 (2002).

¹²K. Matsuda, T. Saiki, S. Nomura, M. Mihara, Y. Aoyagi, S. Nair, and T. Takagahara, Phys. Rev. Lett. **91**, 177401 (2003).

¹³J. R. Guest, T. H. Stievater, G. Chen, E. A. Tabak, B. G. Orr, D. G. Steel, D. Gammon, and D. S. Katzer, Science **293**, 2224 (2001).

¹⁴T. Guenther, C. Lienau, T. Elsaesser, M. Glanemann, V. M. Axt, T. Kuhn, S. Eshlaghi, and A. D. Wieck, Phys. Rev. Lett. **89**, 057401 (2002).

¹⁵W. I. Park, D. H. Kim, S.-W. Jung, and G.-C. Yi, Appl. Phys. Lett. **80**, 4232 (2002).

¹⁶A. Ohtomo, M. Kawasaki, I. Ohkubo, H. Koinuma, T. Yasuda, and Y. Segawa, Appl. Phys. Lett. **75**, 980 (1999).

¹⁷T. Makino, A. Ohtomo, C. H. Chia, Y. Segawa, H. Koinuma, and M. Kawasaki, Physica E (Amsterdam) **21**, 671 (2004).

¹⁸M. Zervos and L.-F. Feiner, J. Appl. Phys. **95**, 281 (2004).

¹⁹M. Zamfirescu, A. Kavokin, B. Gil, G. Malpuech, and M. Kaliteevski, Phys. Rev. B **65**, 161205 (2002).

²⁰S. F. Chichibu, T. Sota, G. Cantwell, D. B. Eason, and C. W. Litton, J. Appl. Phys. **93**, 756 (2003).

²¹D. C. Reynolds, C. W. Litton, D. C. Look, J. E. Hoelscher, B. Clafin, T. C. Collins, J. Nause, and B. Nemeth, J. Appl. Phys. **95**, 4802 (2004).

²²M. Tchoukueu, O. Briot, B. Gil, J. P. Alexis, and R.-L. Aulombard, J. Appl. Phys. **80**, 5352 (1996).

²³T. Wamura, Y. Masumoto, and T. Kawamura, Appl. Phys. Lett. **59**, 1758 (1991).

²⁴A. Zrenner, E. Beham, S. Stuffer, F. Findeis, M. Bichler, and G. Abstreiter, Nature (London) **418**, 612 (2002).

²⁵Z. Yuan, B. E. Kardynal, R. M. Stevenson, A. J. Shields, C. J. Lobo, K. Cooper, N. S. Beattie, D. A. Ritchie, and M. Pepper, Science **295**, 102 (2002).

²⁶T. Kawazoe, K. Kobayashi, S. Sangu, and M. Ohtsu, Appl. Phys. Lett. **82**, 2957 (2003).